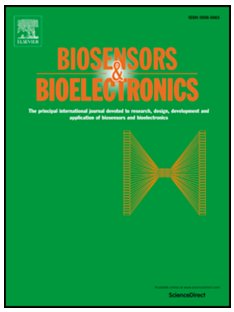

A single-molecule RNA electrical biosensor for COVID-19

Keshani G. Gunasinghe Pattiya Arachchillage, Subrata Chandra, Ajoke Williams, Srijith Rangan, Patrick Piscitelli, Lily Florence, Sonakshi Ghosal Gupta, Juan Artes Vivancos

PII: S0956-5663(23)00566-3

DOI: https://doi.org/10.1016/j.bios.2023.115624

Reference: BIOS 115624

To appear in: *Biosensors and Bioelectronics*

Received Date: 16 May 2023

Revised Date: 17 August 2023

Accepted Date: 18 August 2023

Please cite this article as: Gunasinghe Pattiya Arachchillage, K.G., Chandra, S., Williams, A., Rangan, S., Piscitelli, P., Florence, L., Ghosal Gupta, S., Artes Vivancos, J., A single-molecule RNA electrical biosensor for COVID-19, *Biosensors and Bioelectronics* (2023), doi: https://doi.org/10.1016/j.bios.2023.115624.

Author contributions

Experiments and Initial Data Analysis: KGGPA, SC, AW, SR, PP, LF, SGG
Data analysis, tables and figures: KGGPA, JMAV.
Conceptualization, funding acquisition, project administration, and supervision: JMAV.
All authors contributed to the writing and editing of the manuscript.

Biosensors and Bioelectronics

A single-molecule RNA electrical biosensor for COVID-19

Keshani G. Gunasinghe Pattiya Arachchillage, Subrata Chandra, Ajoke Williams, Srijith Rangan, Patrick Piscitelli, Lily Florence, Sonakshi Ghosal Gupta, Juan Artes Vivancos*

Department of Chemistry, University of Massachusetts Lowell, Lowell, 01854, MA, USA

Abstract

The COVID-19 pandemic shows a critical need for rapid, inexpensive, and ultrasensitive early detection methods based on biomarker analysis to reduce mortality rates by containing the spread of epidemics. This can be achieved through the electrical detection of nucleic acids at the single-molecule level. In particular, the scanning tunneling microscopic-assisted break junction (STM-BJ) method can be utilized to detect individual nucleic acid molecules with high specificity and sensitivity in liquid samples. Here, we demonstrate single-molecule electrical detection of RNA coronavirus biomarkers, including those of SARS-CoV-2 as well as those of different variants and subvariants. Our target sequences include a conserved sequence in the human coronavirus family, a conserved target specific for the SARS-CoV-2 family, and specific targets at the variant and subvariant levels. Our results demonstrate that it is possible to distinguish between different variants of the COVID-19 virus using electrical conductance signals, as recently suggested by theoretical approaches. Our results pave the way for future miniaturized single-molecule electrical biosensors that could be game changers for infectious diseases and other public health applications.

Keywords: COVID-19 detection, single-molecule biosensors, STM-BJ, Biomolecular electronics, STM, Pathogen screening

Highlights

A single-molecule all-electric biosensor for COVID-19 as a proof-of-concept

We target RNA biomarkers for variants and subvariants using scanning tunneling microscopy-assisted break junctions in liquid

The sensor is highly specific and sensitive to one-base differences with single-molecule LOD

We pave the way for future miniaturized single-molecule electrical biosensors for different crucial applications

1. Introduction

The COVID-19 pandemic has taken the world by storm. As of March 2023, there have been reports confirming 681,887,194 cumulative cases of the virus, which have resulted in around 7 million deaths. (Worldometer, 2023) Although the official numbers are widely acknowledged as an underestimate, (Ghodake et al., 2021; Msemburi et al., 2022) it is clear that the pandemic's millions of cases demand an urgent and immediate response. (Yasri and Wiwanitkit, 2022) Due to the high mutation rate of the virus, which has resulted in the constant emergence of new variants, early detection to control spread (Zhang et al., 2022) and finding new treatments and vaccines

for COVID-19 is vital. (Nguyen, 2022). However, the absence of easily accessible rapid detection methods has made therapeutic interventions against COVID-19 difficult. (Ibrahim, 2020) The virus is highly transmissible among humans and it is difficult to keep up with identify and isolate infected individuals. This highlights the urgent need for investments in the development of novel screening methods. (Khan et al., 2020) Efficient early pathogen biosensing methods are crucial and could help contain the spread of the virus and reduce mortality rates. (Nguyen and Kim, 2020; Salian et al., 2021; Suaifan et al., 2017)

In COVID-19 screening, lateral flow assays and real-time (quantitative) polymerase chain reactions (qPCR) have been the gold standards and the main methods used. Lateral flow assay (LFA) is a serological method that plays a role in the control of the COVID-19 pandemic (Zhou et al., 2021) and is fast and effective, but lacks specificity and sensitivity when there is a low concentration of biomarkers (Masterson and Sardar, 2022), and false positives and false negatives limit their clinical use (Hsiao et al., 2021). PCR detection is critical during the early stages of viral infection when the virus multiplies rapidly. qPCR allows for direct amplification, detection (and, potentially, quantification) of pathogen genetic material (Kubina and Dziedzic, 2020). To design an accurate real-time RT-PCR assay, researchers aim to target conserved regions of the virus's genome. The occurrence of false negative results in this type of COVID-19 testing is mainly influenced by the natural progression of the virus within the body, the fluctuating viral load at different anatomical sites, and the methods utilized for sample collection. (Tahamtan and Ardebili, 2020) Traditional diagnostic technologies present challenges in complexity, cost-effectiveness, maintenance, and higher sample preparation time, which can lead to reduced sensitivity, specificity, and limited multiplexing capabilities. (Goud et al., 2021) To address these limitations, there is a growing need for rapid, sensitive, specific, and environmentally friendly biosensors and screening methods. (Abid et al., 2021; Yasri and Wiwanitkit, 2022)

The STM-BJ technique (Xu and Tao, 2003) is up-and-coming for early detection because it can detect individual molecules with high sensitivity and accuracy. (Arachchillage et al., 2021; Li et al., 2018; Lv et al., 2022) This approach is entirely electric and enables highly sensitive detection of specific sequences in complex environments, given that the target sequence is known. (Arachchillage et al., 2021) Single-molecule electrical detection could surpass amplification-based detection limitations since it has higher sensitivity and specificity while avoiding error-prone amplification. (van Kooten et al., 2022) It also has the potential to be more rapid, cost-effective, and accessible compared to established methods such as qPCR (Macchia et al., 2022) since it could be miniaturized, automated, and multiplexed. The Scanning Tunneling Microscopy (STM)-assisted break junctions method (STM- BJ) (Xu and Tao, 2003) has allowed the detection and identification of RNA from E.coli strains at the single molecule level, (Li et al., 2018) cancer RNA biomarkers, (Arachchillage et al., 2023) and could be applied to the early detection of COVID-19.

In this study, we demonstrate a new proof-of-concept approach for the electrical detection of RNA coronavirus biomarkers using the STM-BJ method, starting from the human coronavirus family, down to the SARS-CoV-2 variant and subvariant levels. The results show that we can distinguish between different subvariants of the COVID-19 virus based on the electrical conductance signals obtained from various RNA biomarker sequences hybridized to complementary thiol-modified DNA probes. These results pave the way for the future of miniaturized single-molecule electrical biosensors that could be groundbreaking for COVID-19, other infectious disease detection, and environmental monitoring.

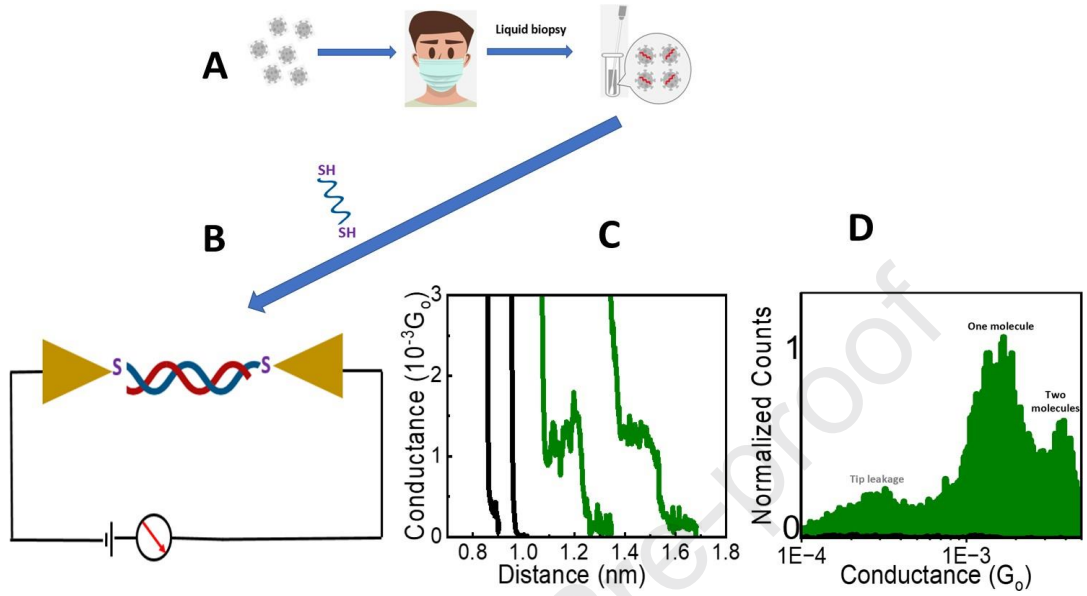

Fig. 1. Electrical detection of coronavirus biomarkers (A) collection of samples using liquid biopsies containing coronavirus biomarkers (B) STM-BJ detection of the hybridized biomarker of interest, resulting in a step in the conductance distance signal (C) Example conductance distance curves. black: control experiment in phosphate buffer, green: Raw data curves from Omicron BA2 RNA experiments. (D) Histogram built from curves with steps, 47 from a total 4504 curves acquired; representing the most probable conductance of the particular molecular junction. ($G_0 = 2e^2/h \approx 77.5$ μS, h: Planck constant, e: electron charge) Bias voltage of 20mV was used for these experiments. (black: Phosphate buffer blank, green: Omicron BA2)

2. Materials and Methods

2.1 Sequence analysis

The Global Initiative on Sharing Avian Influenza Data (GISAID) (*GSAID*, 2023) and the National Center for Biotechnology Information (NCBI) (*NCBI*, 2023) databases were utilized to select and download representative genomes from MERS-CoV, SARS-CoV-2 variants and subvariants, including Alpha, Beta, Delta, Eta, Iota, Kappa, Omicron BA2, Omicron BA5, and Omicron XBB.1.5 to choose specific short sequences to use as DNA probes. All the downloaded representative genomes were used in multiple alignments using the Clustal Omega software (*ClustalOmega*, 2023) to locate the point mutation differences between the targeted variant and the sequences of other known COVID-19 variants. (Figure S1). After analyzing the multiple alignment results, we chose a short sequence conserved for SARS-CoV-2 and other specific sequences for SARS-CoV-2 variants such as Delta, Omicron BA2, and Omicron BA5 (Table S1). The target sequence for all human coronaviruses was chosen from a previously published report. (Abbott et al., 2020) We further checked the specificity of the chosen sequences using the NCBI blast tool (*NCBIBlast*, 2023), comparing them to standard databases and also excluding SARS-CoV-2 (taxid:2697049) (Table S2). It should be noted that it is important to maintain a balance between sequence length and specificity. While the length is important, the primary determining factor is the sequence's specificity, and it is noteworthy that the differences in conductance cannot be predicted. Nonetheless, a specific probe with any detectable conductance is adequate for achieving single-molecule detection. The chosen sequences are then analyzed using the Integrated DNA Technologies (IDT) Oligoanalyzer Tool (*IDT*, 2023) to evaluate their

properties, including the Guanine-Cytosine (GC) content, possible secondary structures, and melting temperatures (Tm) (Table S3). All the Clustal Omega alignment data are available on demand.

2.2 Sample and solution preparation

The thiol-modified DNA probe oligonucleotide sequences and RNA targets were purchased from Biosynthesis Inc. (USA). DNA probes contained C6 spacers and thiol linkers on both 5' and 3' termini in the same strand for electrode binding. The oligonucleotides were delivered in powder form, and after being spun down, they were resuspended in nuclease-free water. After that, the thermal hybridization procedure was carried out by first heating a mixture of the DNA probe and the respective RNA target in a phosphate buffer (100 mM final concentration, pH 7.4) to 80 °C in a water bath and then letting it cool to room temperature for about six hours.

All glassware and Teflon cells were cleaned with piranha solution, prepared by combining 98% sulfuric acid and 30% hydrogen peroxide in a 3:1 v/v ratio (CAUTION: Piranha solution is extremely corrosive and dangerous). Acetone (HPLC plus) and ethyl alcohol (pure) were used to clean all other parts of the STM cell. Before each experiment, the substrate, an Au single crystal (Goodfellow), was electropolished in 0.1 M sulfuric acid using two thin loops of gold wire as electrodes. The Au single crystal was positioned on top of one gold wire loop (the working electrode), and another gold wire loop (the counter electrode) was placed straight above the single crystal, about 0.5 cm away. Working and counter electrodes were connected to the DC power supply, and approximately 10 V and 1 A current was applied for a duration of thirty seconds until the top layer of the Au single crystal turned orange. The oxidized Au single crystal was then rinsed about five times with deionized water. Following a three-minute soak in a 1 M hydrochloric acid solution, the Au single crystal changed color from orange back to shiny gold. The crystal was again rinsed with deionized water about three times. Finally, the clean Au single crystal was air-dried before being annealed for about 1 minute using a butane flame.

A 100 mM phosphate buffer was used for all experiments. Disodium hydrogen monophosphate and sodium dihydrogen phosphate were used to prepare the 100 mM phosphate buffer (pH 7.4) with deionized water. Then the buffer solution was filtered with 20 nm pore size filters (Whatman Anotop 25 plus) before experiment use. Chemicals such as acetone (HPLC plus), ethyl alcohol (pure), sulfuric acid, hydrochloric acid, disodium hydrogen monophosphate, and sodium dihydrogen phosphate were purchased from Sigma-Aldrich. In the experiments, we utilized the following instruments and equipment: the Eppendorf Centrifuge 5425 (frequency: 50-60 Hz, Max speed: 15060 rpm), Scilogex D1008 Mini-Centrifuge, Corning LSE vortex mixer, and Zeba™ Spin Desalting Columns 7K MWCO.

2.3 STM-Break junction measurements on DNA:RNA hybrids for coronavirus biomarkers

All experiments were done at room temperature with a Pico-STM Molecular Imaging head connected to a Digital Instruments Nanoscope IIIa controller. The 10 nA/V preamplifier and bias voltages of 100 mV and 20 mV were used for experiments. To ensure that the cell was free of contaminants, a control phosphate buffer experiment (see Fig. 1D black histogram, and Fig. 2F black histogram) was conducted before each experiment. A small sample volume was added to the STM cell in a typical DNA:RNA hybrid experiment to achieve final concentrations in the μM range for the conductance measurements. Thiol groups in DNA probes were protected by disulfide bonds, and TCEP (Tris (2-carboxyethyl) phosphine) was used to reduce the disulfide bond, resulting in free thiol groups that could be attached to the Au surface and the Au tip. Over a wide pH range, TCEP completely and selectively reduces disulfides in less than 5 minutes at room temperature. (*TCEPReduction*, 2023)

The STM tip was made by cutting 0.25 mm gold wire (Goodfellow) at about a 45° angle and coating it with Apiezon wax (Apiezon products). Waxing the tip minimizes the exposed surface area, thereby reducing faradaic current leakage in solution. By using the STM-BJ (Xu and Tao, 2003) approach, the STM tip was repeatedly brought into and out of contact with the Au substrate, creating a tip-substrate gap that enables a molecule to bridge in the nanometer length. A

customized LabVIEW (Hihath & Tao, 2008) program was used to control the movement of the STM tip and gather data. During a single experiment, approximately four thousand current-distance traces were recorded. When a molecule was bound between the Au tip and Au substrate, we observed steps in some traces (see Fig. 1B).

2.4 Statistical analysis of STM-BJ data

The thousands of collected data were analyzed using a custom LabVIEW program. (Hihath & Tao, 2008) This program logarithmically bins each current-distance trace that is recorded. The algorithm scans through all the curves and selects those that meet specific criteria, typically having more than a certain number of counts. This selection process was further improved through manual refinement, excluding noisy curves and retaining only those with distinct plateaus. All of those selected curves with steps were added together to generate a semi-logarithmic conductance histogram representing the most probable conductance of the particular molecular junction. Gaussian fitting was employed to determine the peak position and the counts were normalized to the most prominent peak count of each histogram. In general, 4000 curves are sufficient to observe a prominent conductance peak, even if the raw histogram (without smoothing or averaging) appears noisy or spiky.

2.5 In situ hybridization experiments for Omicron BA5 subvariant

We conducted *in situ* hybridization experiments on an Omicron BA5 RNA sample to assess the specificity of this biosensing approach. We started with a buffer control experiment (see Fig. 2F black histogram) and then injected the thiolated DNA probe designed for the SARS-CoV-2 Omicron BA5 subvariant into the same STM cell in a second control experiment (see the histogram in figure S2). Finally, we added the SARS-CoV-2 Omicron BA5 subvariant's complementary RNA target to the same cell. Following each experiment, we used the same statistical analysis procedure described above to obtain the most probable conductance histogram for each case.

3. Results and Discussion

3.1 proof of concept COVID-19 single molecule electrical biosensor

STM-BJ measurements have previously shown that the conductance of several nucleic acids, including double-stranded (ds) DNA, ds RNA, and RNA:DNA hybrids can be measured at the single-molecule level (Chandra et al., 2022; Hihath et al., 2005; Lewis et al., 1997; Li et al., 2016a, 2018; Murphy et al., 1993; Xiang et al., 2015). These reports demonstrate that the charge transport processes in oligonucleotides are sensitive to sequence and structure, (Artés et al., 2015; Li et al., 2016b,a) as well as single-base mismatches (Hihath et al., 2005; Li et al., 2018), length, and environmental effects (Li et al., 2018). This means that this method should be suitable for detecting COVID-19 RNA biomarkers down to a single base mismatch resolution. Fig. 1A shows a schematic diagram for the detection method, in which a liquid biopsy sample containing the RNA target biomarker from COVID-19 is targeted with specific dithiol-modified DNA probes for molecular-level recognition and electrical detection. Our RNA target sequences correspond to the family of human coronaviruses (including all highly pathogenic coronaviruses such as SARS-CoV, MERS-CoV, and SARS-CoV-2 (Grellet et al., 2022; Machitani et al., 2020)), the Delta variant, and two Omicron sub-variants (BA2 and BA5). An important reason for targeting RNA is that the COVID-19 virus has a positive sense single-strand RNA genome, which can function as mRNA directly translated into viral proteins (Amarilla et al., 2021; Machitani et al., 2020). We also target RNA sequences because RNA transcription naturally amplifies RNA during the interphase of the cell, simplifying the approach by eliminating the need to convert RNA into complementary DNA (cDNA) before detection (Li et al., 2018). Specific DNA probes hybridize with the target RNA sequences and the resulting DNA:RNA hybrid can bind to the STM electrodes throughits thiol groups (Fig. 1B), resulting in the formation of a biomolecular electronics circuit and allowing the measurement of an electrical fingerprint for the DNA:RNA hybrid. In STM-BJ experiments, an atomically sharp gold tip is brought into and out of contact with the gold substrate while conductance measurements are monitored. Fig. 1C shows molecular

conductance steps (conductance-distance curves) after forming molecular junctions between the two STM electrodes. No steps are present in the control experiment, as no molecules are bound between the two gold electrodes. We accumulate single-molecule electrical measurement data for statistical analysis by repeating the formation of the junction several thousands of times, resulting in a conductance histogram representing the most probable conductance value for the particular DNA:RNA hybrid (Fig. 1D ($G_0 = 2e^2/h$ 77.5 μS; G_0: quantum conductance, h: Planck constant, e: electron charge). The second conductance peak in Fig. 1, present at a value double that of the first conductance, indicates two DNA:RNA molecules trapped in parallel. Previous experimental studies have shown that the DNA:RNA hybrid conductance is in the 10^{-4} - 10^{-3} G_0 range, consistent with our data. (Arachchillage et al., 2023;Chandra et al., 2022; Li et al., 2016a,b, 2018) Also, recent theoretical approaches propose that the molecular conductance of nucleic acids from different SARS- CoV-2 variants should be in the 10^{-7} G_0 - 10^{-4} G_0 range, in the same range as our findings. (He et al., 2022, 2023) Small faradaic (non-tunneling) currents and the noise of the current amplifier result in a tip leakage feature in the histogram, representing the lower conductance limit typical in these measurements in the buffer. (Artés et al., 2015)

3.2 Electrical detection of biomarkers from SARS-CoV-2 variants and subvariants

After bioinformatic analysis, we use the STM-BJ method (Xu and Tao, 2003) to measure the electrical fingerprints of individual coronavirus RNA sequences. This biosensing strategy allows us to distinguish different coronavirus variants with different lengths and sequences. We obtain conductance histograms for different variants of coronaviruses as discussed above; histogram A in Fig. 2 shows the single-molecule conductance for a sequence that is conserved in all human coronaviruses, such as SARS-CoV, MERS- CoV, SARS-CoV-2, etc... Histogram B shows the conductance histogram for a conserved sequence specific for SARS-CoV-2. In Fig. 2, C, D, and E show conductance histograms for the SARS-CoV-2 Delta variant, subvariant specific sequences Omicron BA2 and BA5, respectively. Table 1 presents the average conductance values for each variant of the coronavirus and subvariant sequence, obtained from three independent STM-BJ experiments for each case. These results demonstrate that we can detect individual coronavirus biomarkers and distinguish them from each other through different specific oligonucleotide DNA probes.

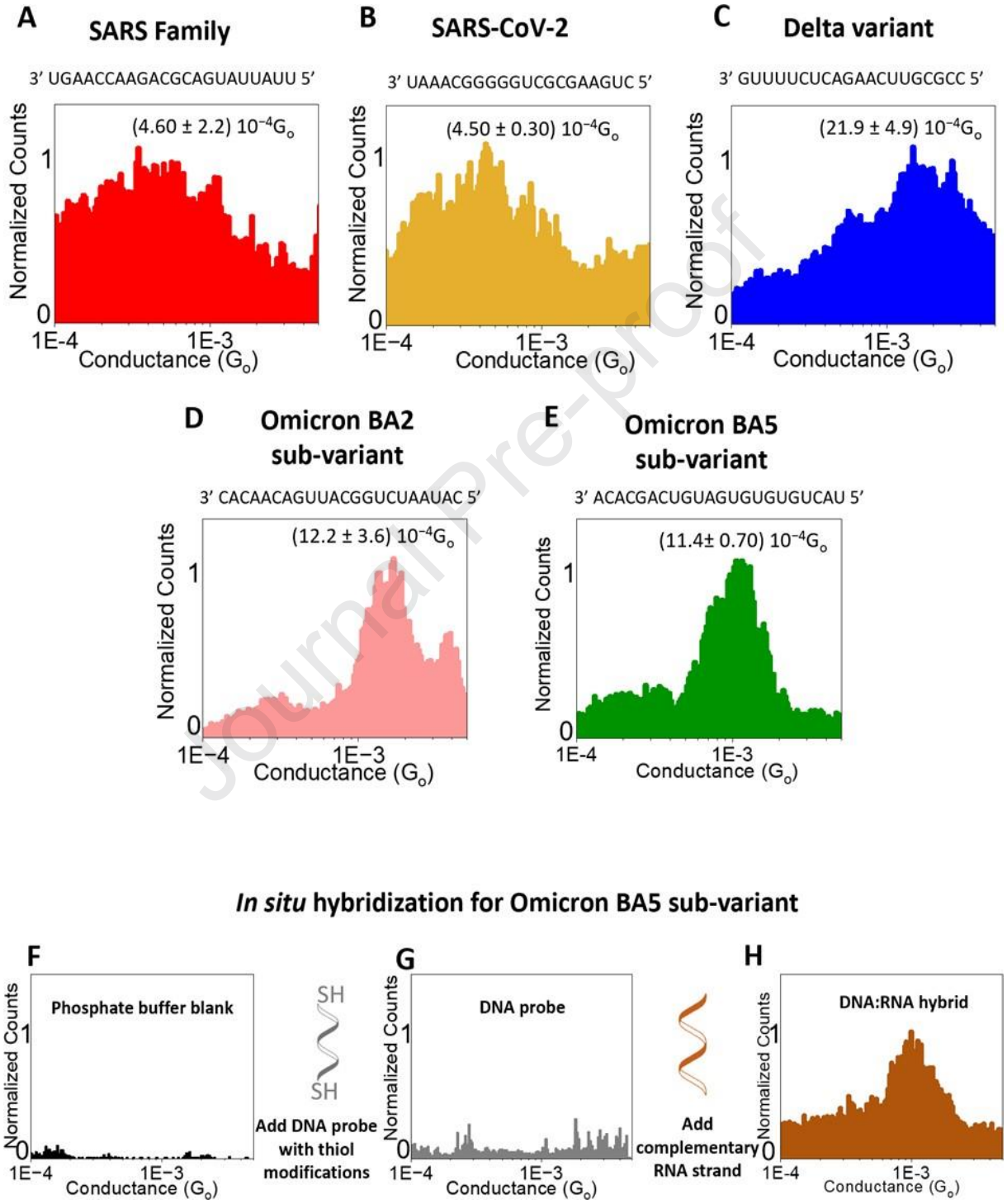

Fig. 2. Electrical detection of biomarkers from SARS-CoV-2 variants and subvariants (A) conductance histogram for SARS-family (90 from a total 13142 curves acquired) (B) conductance histogram for SARS-CoV-2 (127 from a total 4085 curves acquired) (C) conductance histogram for Delta (142 from a total 6119 curves acquired) (D) conductance histogram for Omicron BA2 (47 from a total 4504 curves acquired) (E) conductance histogram for Omicron BA5 (57 from a total 5469 curves acquired) (F), (G), (H) In situ hybridization for Omicron BA5 sub-variant (F) conductance histogram for blank phosphate buffer (2 from a total 1041 curves acquired) (G) conductance histogram for Omicron BA5 DNA probe (1 from a total 3059 curves acquired) (H) conductance histogram for Omicron BA5 DNA:RNA hybrid (92 from a total 9956 curves acquired). These electrical conductance measurements enable the differentiation of various coronavirus variants with different lengths and sequences. (Bias voltage of 100 mV was used for SARS-family, SARS-CoV-2, and Delta experiments. Bias voltage of 20 mV was used for Omicron BA2 and Omicron BA5 experiments)

Table 1: Statistics of single-molecule conductance for coronavirus biomarkers: average and standard deviations for three different single-molecule conductance experiments, from at least 4000 acquired curves. 100 mV bias was used for the SARS family, SARS-CoV-2, and Delta experiments. 20 mV bias was used for the Omicron BA2 and Omicron BA5 experiments ($G_0 = 2e^2/h \approx 77.5$ μS; G_0: quantum conductance, h: Planck constant, e: electron charge)

	SARS Family 22nt	SARS- CoV-2 Conserved 20nt	Delta Variant 20nt	Omicron BA2 Variant 22nt	Omicron BA5 Variant 22nt
RNA Sequence	3'UGAACC AAGAC GCAGUAU UAUU5'	3'UAAAC GGGGGU CGCGAAGU C5'	3'GUUUU CUCAGA ACUUGC GCC5'	3'CACAA CAGUUA CGGUCUAA UAC5'	3'ACACG ACUGUA GUGUGUGU CAU5'
Conductance ($10^{-4}G_0$)	4.60 ± 2.2	4.50 ± 0.30	21.9 ± 4.9	12.2 ± 3.6	11.4 ± 0.70

After demonstrating the possibility of electrical detection of individual coronavirus biomarkers, we perform *in situ* hybridization experiments for an example RNA target sequence, the SARS-CoV-2 Omicron BA5 subvariant. Fig. 2F, G, and H show the results of the *in situ* hybridization experiments, where the black low-intensity histogram is the phosphate buffer (pH 7.4) control experiment that shows no conductance peaks. Then, we injected the thiolated DNA probe designed for the SARS-CoV-2 Omicron BA5 subvariant into the STM cell in a second control experiment, resulting in a similar featureless conductance histogram, with no conductance peaks (gray low intensity histogram in Fig. 2G). Finally, we added the complementary RNA target of the SARS-CoV-2 Omicron BA5 subvariant and measured a conductance peak around 11×10^{-4} G_0, matching the green histogram shown in Fig. 2E. The charge transport process at this energy is mediated primarily by base stacking in the double helix and is strongly influenced by the delocalization length through the bases (Artés et al., 2015; Li et al., 2016b; Xiang et al., 2015). Therefore, it is necessary to have both the thiolated specific probe binding the electrodes and the RNA target present to enable a conductance pathway that closes the biomolecular electronics circuit and thus produces an electrical fingerprint.

These results show that the screening method used in this study can distinguish between variants of SARS-CoV-2, which is essential for early screening and diagnosis. Our findings are consistent with recent theoretical approaches that propose COVID detection using conductance variation caused by single nucleotide differences between SARS-CoV-2 and its five variants of concern (Alpha, Beta, Gamma, Delta, and Omicron) (He et al., 2022, 2023). This type of electrical detection applications have reported lower limits of detection, often in the aM range (Li et al., 2018; Arachchillage et al., 2023) or even at the level of individual molecules,(Arachchillage et al., 2023) and offers impressive specificity in single-base mismatch detection.(Li et al., 2018; Arachchillage et al., 2023) In comparison, the "BinaxNOW COVID-19 Ag Card," the first FDA-approved rapid antigen test (an LFA immunoassay), (Filchakova et al., 2022) has a detection limit of approximately 4.04×10^4 to 8.06×10^4 copies per swab. (Filchakova et al., 2022; Perchetti et al., 2021) Additionally, RT-PCR, the golden standard, has an average limit of detection of 9.2 copies per reaction with high specificity. (Filchakova et al., 2022)

Different SARS-CoV-2 variants may exhibit varying

degrees of virulence and susceptibility to vaccines; therefore the ability to predict emerging variants of dangerous pathogens such as SARS-CoV-2 can be a game changer in monitoring and combating epidemics and pandemics. Consequently, anticipating new variants can guide public health policies and reduce the impact of outbreaks. With this biosensing method, the combination of the data gathered provides a framework for designing an effective strategy to detect and identify emerging pathogen variants for this pandemic by tracking the distribution pattern of the conductance measurements, when these measurements can be automatized and parallelized into several channels. Furthermore, the concept could easily be extrapolated to other infectious diseases or other applications.

The current study presents a fully electrical proof-of-concept nanobiosensor aimed at detecting and distinguishing COVID-19 and its various variants and sub-variants. The validation of this concept will require conducting final proof-of-concept demonstrations using patient samples or samples from biobanks. This is essential to address the challenges posed by complex media, as some relevant RNA detection experiments in complex were already demonstrated in the literature. (Veselinovic et al., 2019) Moving for- ward, future developments should concentrate on creating affordable, highly sensitive, and user-friendly devices while overcoming miniaturization hurdles and exploring possibilities for parallelization and automation. These engineering and experimental challenges may also play a role in advancing biomolecular electronics fundamental research. Developing new data analysis approaches, such as the application of machine learning to analyze conductance histograms, will enhance the applicability and automatization of these technologies. (Arachchillage et al., 2021) As we advance in biosensor research, sustainability should remain a clear consideration in the design and development of these sensors to benefit human well-being without feeding other potential crises. (Williams et al., 2023)

4. Conclusion

We demonstrate a direct electrical biosensor to measure the conductance of coronavirus biomarkers. This sensor is capable of single-molecule detection and is highly sensitive to different sequences, allowing for the distinction between different variants and subvariants. This biosensor also has the potential to be automated and parallelized in the future and the potential to detect and identify upcoming strains. This biosensing strategy's versatility extends to detecting various pathogen types and also offers the potential for automated electrical environmental monitoring.

Acknowledgment

We acknowledge support from the NSF (Award Number 2027530) and from UMass Lowell (the Immersive Scholars program, the Wong research award 2020, and the Kennedy College of Sciences Giants fund 2021). Au- thors also acknowledge contributions from R. Kapala from Lowell Precision Manufacturing in the design and fabrication of a fluid STM cell and useful discussions with Prof. F. Chain.

Additional information

All data and methods are available in the main text, the supplementary materials, or will be provided on demand.

Author contributions

Experiments and Initial Data Analysis: KGGPA, SC, AW, SR, PP, LF, SGG

Data analysis, tables, and figures: KGGPA, JMAV.

Conceptualization, funding acquisition, project administration, and supervision: JMAV.
All authors contributed to the writing and editing of the manuscript.

Competing interests

The authors declare that they have no competing interests nor any other interests.

Supplementary Information

Supplementary information for this article can be found online at …

References

Abid, S.A., Muneer, A.A., Al-Kadmy, I.M., Sattar, A.A., Beshbishy, A.M., Batiha, G.E.S., Hetta, H.F., 2021. Life Sci. 273, 119117.

Amarilla, A.A., Sng, J.D., Parry, R., Deerain, J.M., Potter, J.R., Setoh, Y.X., Rawle, D.J., Le, T.T., Modhiran, N., Wang, X., et al., 2021. Nat. Commun 12, 3431.

Arachchillage, K., Chandra, S., Williams, A., Piscitelli, P., Pham, J., Castillo, A., Florence, L., Rangan, S., Artes Vivancos, J., 2023. Sci. Rep. 13, 12428.

Arachchillage, K.G.G.P., Chandra, S., Piso, A., Qattan, T., Vivancos, J.M.A., 2021. J Mater Chem B 9, 6994–7006.

Artés, J.M., Li, Y., Qi, J., Anantram, M., Hihath, J., 2015. Nat. Commun 6, 8870.

Chandra, S., Arachchillage, K.G.G.P., Kliuchnikov, E., Maksudov, F., Ayoub, S., Barsegov, V., Vivancos, J.M.A., 2022. Nanoscale 14, 2572–2577.

Filchakova, O., Dossym, D., Ilyas, A., Kuanysheva, T., Abdizhamil, A., Bukasov, R., 2022. Talanta 244, 123409.

Ghodake, G.S., Shinde, S.K., Kadam, A.A., Saratale, R.G., Saratale, G.D., Syed, A., Elgorban, A.M., Marraiki, N., Kim, D.Y., 2021. Biosens. Bioelectron. 177, 112969.

Goud, K.Y., Reddy, K.K., Khorshed, A., Kumar, V.S., Mishra, R.K., Oraby, M., Ibrahim, A.H., Kim, H., Gobi, K.V., 2021. Biosens. Bioelectron. 180, 113112.

Grellet, E., Goulet, A., Imbert, I., 2022. J. Biol. Chem. , 101923.

He, L., Xie, Z., Long, X., Zhang, C., He, C., Zhao, B., Qi, F., Zhang, N., 2022. Process Biochem 121, 656–660.

He, L., Xie, Z., Long, X., Zhang, C., Ma, K., She, L., 2023. Biophys. Chem., 107013.

Hihath, J., Xu, B., Zhang, P., Tao, N., 2005. Proc. Natl. Acad. Sci. U.S.A. 102, 16979–16983.

Hihath, J., & Tao, N. (2008). Nanotechnology, 19(26), 265204.

Hsiao, W.W.W., Le, T.N., Pham, D.M., Ko, H.H., Chang, H.C., Lee, C.C., Sharma, N., Lee, C.K., Chiang, W.H., 2021. Biosensors 11, 295.

Ibrahim, N.K., 2020. J. Infect. Public Health 13, 1630–1638.

Khan, M., Hasan, M., Hossain, S., Ahommed, M., Daizy, M., 2020. Biosens. Bioelectron. 166, 112431.

van Kooten, X.F., Rozevsky, Y., Marom, Y., Sadeh, E.B., Meller, A., 2022. Nanoscale 14, 4977–4986.

Kubina, R., Dziedzic, A., 2020. Diagnostics 10, 434.

Lewis, F.D., Wu, T., Zhang, Y., Letsinger, R.L.,Greenfield, S.R., Wasielewski, M.R., 1997. Science 277, 673–676.

Li, Y., Artés, J.M., Demir, B., Gokce, S., Mohammad, H.M., Alangari, M., Anantram, M.P., Oren, E.E., Hihath, J., 2018. Nat. Nanotechnol. 13, 1167–1173.

Li, Y., Artés, J.M., Hihath, J., 2016b. Small 12, 432–437.

Li, Y., Artes, J.M., Qi, J., Morelan, I.A., Feldstein, P., Anantram, M.P., Hihath, J., 2016a. J. Phys. Chem. Lett. 7, 1888–1894.

Lv, S.L., Zeng, C., Yu, Z., Zheng, J.F., Wang, Y.H., Shao, Y., Zhou, X.S., 2022. Biosensors 12, 565.

Macchia, E., Kovács-Vajna, Z.M., Loconsole, D., Sarcina, L., Redolfi, M., Chironna, M., Torricelli, F., Torsi, L., 2022. Sci. Adv. 8, eabo0881.

Machitani, M., Yasukawa, M., Nakashima, J., Furuichi, Y., Masutomi, K., 2020. Cancer Sci. 111, 3976–3984.

Masterson, A.N., Sardar, R., 2022. ACS Appl. Mater. Interfaces 14, 26517– 26527.

Msemburi, W., Karlinsky, A., Knutson, V., Aleshin-Guendel, S., Chatterji, S., Wakefield, J., 2022. Nature, 1–8.

Murphy, C., Arkin, M., Jenkins, Y., Ghatlia, N., Bossmann, S., Turro, N., Barton, J., 1993. Science 262, 1025–1029.

Nguyen, K.V., 2022. Nucleosides Nucleotides Nucleic Acids 41, 778–814. Nguyen, Q.H., Kim, M.I., 2020. TrAC, Trends Anal. Chem. 132, 116038.

Perchetti, G.A., Huang, M.L., Mills, M.G., Jerome, K.R., Greninger, A.L., 2021. J. Clin. Microbiol. 59, 10–1128.

Salian, V.S., Wright, J.A., Vedell, P.T., Nair, S., Li, C., Kandimalla, M., Tang, X., Carmona Porquera, E.M., Kalari, K.R., Kandimalla, K.K., 2021. Mol. Pharm. 18, 754–771.

Suaifan, G.A., Alhogail, S., Zourob, M., 2017. Biosens. Bioelectron. 92, 702– 708.

Tahamtan, A., Ardebili, A., 2020. Expert review of molecular diagnostics 20, 453–454.

Veselinovic, J., Alangari, M., Li, Y., Matharu, Z., Artés, J.M., Seker, E., Hihath, J., 2019. Electrochim. Acta 313, 116–121.

Williams, A., Regalado Aguilar, J., Arachchillage, K., Chandra, S., Rangan, S., Gupta, S., Blestel, E., , Gupta, S., Artes Vivancos, J., 2023. Submitted, ACS Sustain. Chem. Eng.

Worldometer, 2023. https://www.worldometers.info/coronavirus/. Accessed: 2023-05-11.

Xiang, L., Palma, J.L., Bruot, C., Mujica, V., Ratner, M.A., Tao, N., 2015. Nat. Chem. 7, 221–226.

Xu, B., Tao, N.J., 2003. Science 301, 1221–1223.

Yasri, S., Wiwanitkit, V., 2022. Sens. Int. , 100171.

Zhang, W., Liu, N., Zhang, J., 2022. Biosens. Bioelectron. 201, 113944.

Zhou, Y., Wu, Y., Ding, L., Huang, X., Xiong, Y., 2021. TrAC, Trends Anal. Chem. 145, 116452.

Web References

ClustalOmega. (2023). https://www.ebi.ac.uk/Tools/msa/clustalo/

GSAID. (2023). https://gisaid.org/

IDT. (2023). https://www.idtdna.com/calc/analyzer

NCBI. (2023). https://www.ncbi.nlm.nih.gov/nuccore/?term=

NCBIBlast. (2023). https://blast.ncbi.nlm.nih.gov/Blast.cgi?PROGRAM=blastn&PAGE_TYPE=BlastSearch&LINK_LOC=blasthome

TCEPReduction. (2023). https://www.biosyn.com/tew/instruction-of-reduction-reaction-using-tcep.aspx

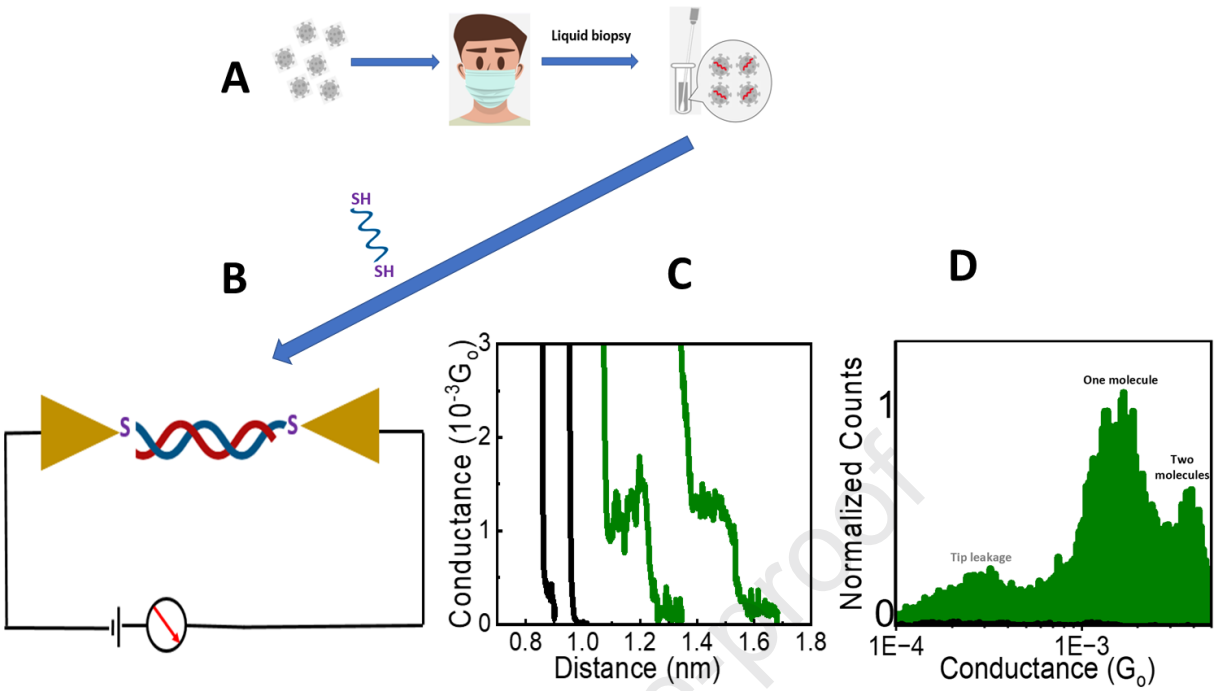

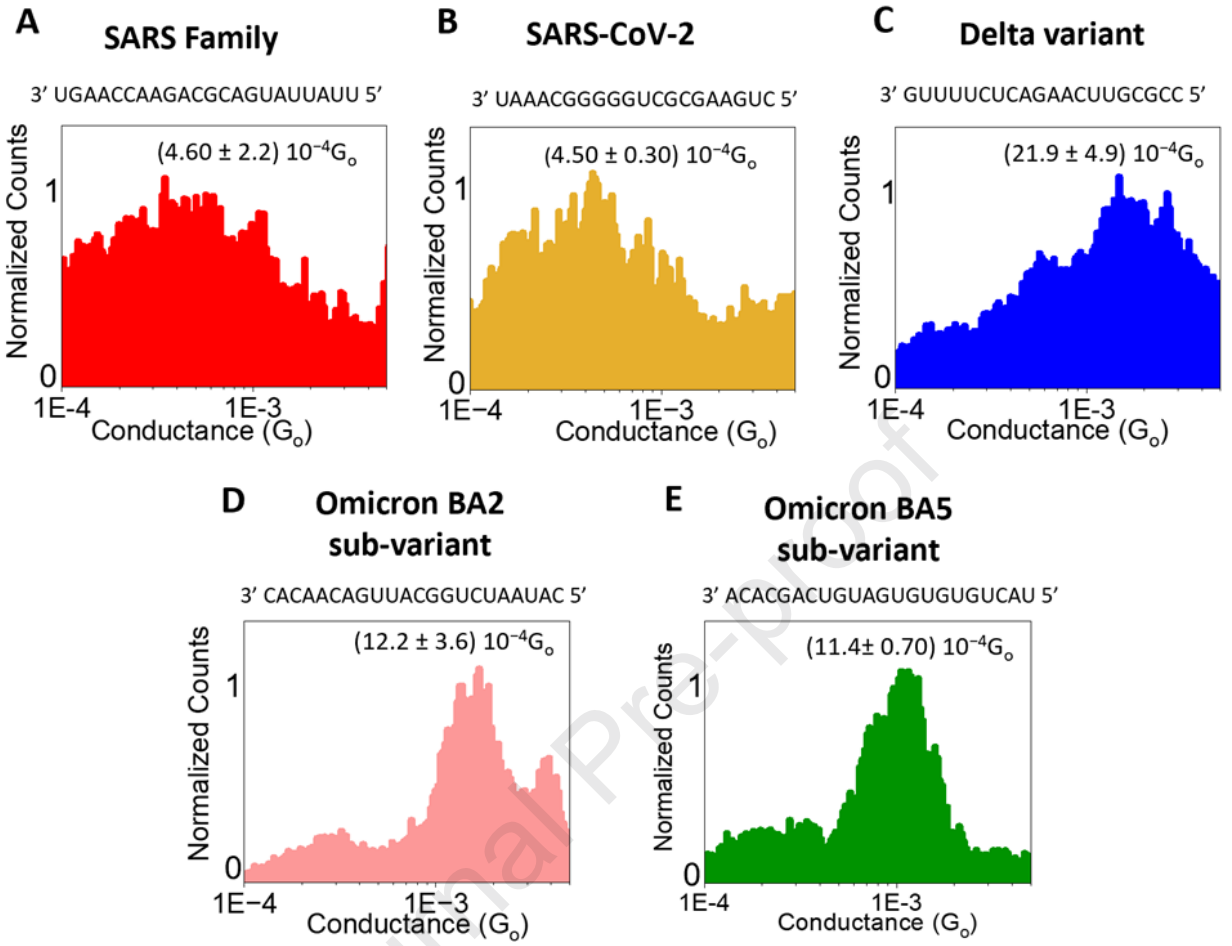

***In situ* hybridization for Omicron BA5 sub-variant**

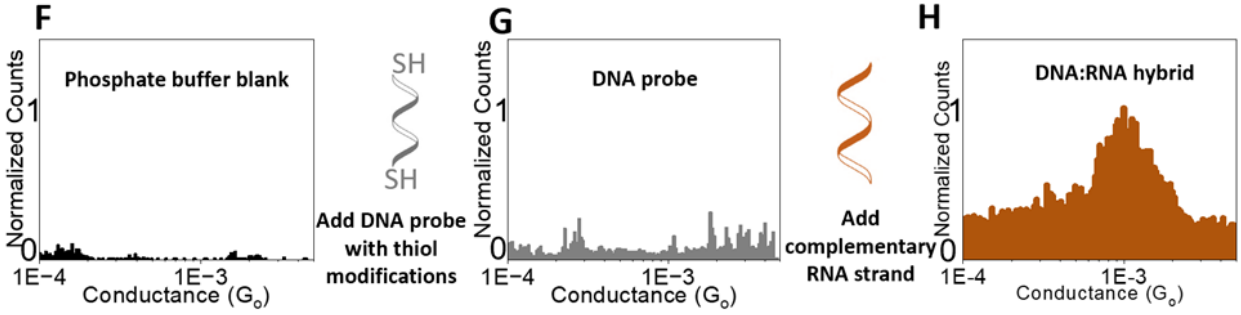

Declaration of interests

☐ The authors declare that they have no known competing financial interests or personal relationships that could have appeared to influence the work reported in this paper.

☒ The authors declare the following financial interests/personal relationships which may be considered as potential competing interests:

Juan Artes Vivancos reports financial support was provided by National Science Foundation.